Theory of singlet-ground-state magnetism: Application to field-induced transitions in $CsFeCl_3$ and $CsFeBr_3$

Per-Anker Lindgård
Solid State Physics Department, Risø National Laboratory, DK-4000 Roskilde, Denmark

Burkhard Schmid
Institut Laue-Langevin, F-38042 Grenoble Cedex 9, France
(Received 7 June 1993)

In the singlet ground-state systems $CsFeCl_3$ and $CsFeBr_3$ a large single-ion anisotropy causes a singlet ground state and a doubly degenerate doublet as the first excited states of the Fe^{2+} ion. In addition the magneteic interaction is anisotropic being much larger along the z axis than perpendicular to it. Therefore, these quasi-one-dimensional magnetic model systems are ideal to demonstrate unique correlation effects. Within the framework of the correlation theory we derive the expressions for the excitation spectrum. When a magnetic field is applied parallel to the z axis both substances have phase transitions to commensurate long-range order. In $CsFeCl_3$ this transition is preceded by two transitions to incommensurate structures. The calculated fluctuation effects can indeed explain the experimentally detected incommensurate order in $CsFeCl_3$, and also the absence of that in $CsFeBr_3$. A sophisticated numerical and graphical method leads to a self-consistent determination of the induced magnetization and the quadrupole moment as well as to the determination of the excitation spectrum for $CsFeBr_3$ and $CsFeCl_3$ as a function of the magnetic field. For magnetic fields below the phase transition the experimental data can be excellently described by the self-consistent random-phase approximation results. For magnetic fields near the critical magnetic field only qualitative conclusions can be obtained. Numerical results for the critical scattering, the correlation lengths, and the specific heat, which are based on the analysis of the first-moment frequency, support the supposition that the field-induced transition is approaching a second-order phase transition.

I. INTRODUCTION

The static and dynamic properties of crystal-field systems with weak interactions are examples of very general problems in physics. It is the problem of interacting objects with internal degrees of freedom. In particular the systems which have a nonmagnetic singlet ground state (SGS) have attracted interest.[1] Here one refers to the mean-field ground state. The true ground state in these systems is basically unknown; therefore a theory of magnetic excitations encounters the same difficulties as the theory of antiferromagnets. Hybrid mean-field and crystal-field theories were developed by several authors.[2] A self-consistent theory for systems strongly influenced by crystal fields using standard basis operators and the random-phase approximation (RPA) was developed by Hayley and Erdös.[3] This was formally extended in the correlation theory (CT),[4] which includes the effects of pair correlations. A realistic self-consistent RPA calculation was previously performed for Pr (Ref. 5) and shown to accurately describe the softening of the most critical mode as a function of temperature. Using the correlation theory for Pr the line-shape behavior including the possibility for a dynamical central peak in a SGS was discussed.[6] A central peak is found experimentally[7] in the rather complicated Pr system, but its origin is not yet quite clear. The problem is that the wave vectors for the soft mode and the central peak are close, but they do not coincide exactly as would be expected from simple theories. A preliminary analysis[8] for the case of planar magnets suggested that a pronounced central peak in the line shape for the soft mode could occur in the strongly correlated systems, such as $CsFeCl_3$. The theory for different directions of the ordered moment in the ordered phases was developed in the context of martensitic transformations.[9] It is convenient to follow this notation here and simplify it to the case of one sublattice.

In this paper we are mainly interested in studying the applications of the self-consistent theories to the ideal singlet-ground-state systems $CsFeBr_3$ and $CsFeCl_3$. They are both $S=1$ magnets with strong antiferromagnetic and ferromagnetic correlated chains, respectively, coupled antiferromagnetically in a triangular pattern.[10,11] The anisotropy energy is of the form DS_z^2 and is large enough to prevent three-dimensional (3D) magnetic ordering in the limit of zero temperature. Nevertheless, the magnetic excitations show an interesting behavior. Even in the nonordered phase there exist well-defined magnetic excitations which originate from single-ion excitations to the excited doublet. However, by applying a magnetic field perpendicular to the hexagonal plane a 3D magnetic order can be induced. For $CsFeBr_3$ this leads to a frustrated 120° structure in the hexagonal plane. The phase transition is driven by mode softening with the ordering vector $\mathbf{Q}$ at the K point in the reciprocal space. With no external field the minimum of the dispersion in $CsFeCl_3$ is

displaced from the K point.[12] This may be explained by the influence of dipolar forces[13] which split the doubly degenerate exciton modes except at the K point. In principle this effect should also be observable in $CsFeBr_3$. It was not observed in $CsFeBr_3$.[14] When an external field along the chain direction is applied, magnetic ordering occurs with an incommensurate $\mathbf{Q}$ close to the $\mathbf{K}$ point in $CsFeCl_3$.[12] In this case dipolar forces cannot explain the effect because the modes are already split by the magnetic field and the RPA dispersion relation has the minimum at the $\mathbf{K}$ point for large fields. A possible cause of incommensurability is that the exchange interactions are of long range. For physical reasons there is no basis for expecting the range to be different for $CsFeBr_3$ and $CsFeCl_3$. The dispersion relation for moderate fields consequently shows no indication of the minimum displaced from the $\mathbf{K}$ point for $CsFeCl_3$. However, Lindgård[15] has shown that correlation effects qualitatively give an explanation for the experimental results even when dipolar forces are neglected. This will be further studied in this paper.

The use of thermal averages including the crystal field only gives rise to RPA theory, which is not fully self-consistent. A fully self-consistent generalization of the theory—the correlation theory—has been developed in terms of the generalized angular momentum operators, the so called Raccah or Stevens tensor operators.[4] The CT has, like the RPA theory, the virtue of being simple and applicable to many systems, including disordered systems, because short-range order effects are taken into account by including pair correlations self-consistently in both static and dynamic properties.

In the following we introduce the model Hamiltonian and then discuss the excitation spectrum, the free energy and self-consistently calculated spin-spin correlation functions by means of CT. The inclusion of correlation effects as a function of magnetic fields H^α perpendicular to and within the hexagonal plane will be discussed.

II. MODEL HAMILTONIAN

For discussing the magnetic properties of the SGS we consider the general, Fourier transformed Hamiltonian

$$\mathcal{H}=-\frac{1}{2}\sum_{\mathbf{q}}\{J_q^{\parallel}S_q^zS_{-q}^z+J_q^{\perp}S_q^+S_{-q}^-+K_qS_q^+S_{-q}^+ +K_q^*S_q^-S_{-q}^-\} +\sum_{\mathbf{R}}\{DS^{z2}(\mathbf{R})-H_{\parallel}S^z(\mathbf{R})-H_{\perp}S^x(\mathbf{R})\}\ . \tag{1}$$

$J_{\mathbf{q}}^{\parallel}$ and $J_{\mathbf{q}}^{\perp}$ denote the Fourier transformed exchange integrals along and perpendicular to the chains, respectively. $K_{\mathbf{q}}$ stands for the Fourier transform of the anisotropic part of the dipolar interaction. If dipolar forces are neglected $J_{\mathbf{q}}^{\parallel}=J_{\mathbf{q}}^{\perp}$ and $K_{\mathbf{q}}=0$. We define the Fourier transforms as $J_{\mathbf{q}}=\sum_{\mathbf{R}}J_{\mathbf{R}}\exp(i\mathbf{q}\cdot\mathbf{R})$. In order to discuss the two possibilities—the external field perpendicular and parallel to the z direction, respectively—we rewrite the Hamiltonian (1) in the following form, neglecting the dipolar interaction

$$\mathcal{H}=-\frac{1}{2}\sum_{\mathbf{q}}J_{\mathbf{q}}\mathbf{S}_{\mathbf{q}}\cdot S_{-\mathbf{q}}+\sum_i(DS_i^{z2}-H_{\parallel}S_i^z)-H_{\perp}\sum_i S_i^x\ . \tag{2}$$

We define the following quadrupolar operators

$$\hat{Q}_x=2(S_z^2-S_y^2),\quad \hat{Q}_y=2(S_z^2-S_x^2)\ ,$$
$$\hat{Q}_z=2(S_x^2-S_y^2),\quad \hat{L}^x=(S^zS^y+S^yS^z)\ , \tag{3}$$

with the remaining $\hat{L}^\alpha$, $\alpha=x,y,z$, obtained by cyclic permutations. The correct treatment of the anisotropy term requires the introduction of these operators. The commutators between the spin and the quadrupolar operators give again quadrupolar operators, and commutators between two quadrupolar operators give spin operators for $S=1$, as can easily be checked.

III. THE EXCITATION SPECTRUM

A. Overview of the general correlation theory

The aim of CT is to calculate both the static and dynamic properties self-consistently, including correlation effects in a mode-mode coupling approximation. A detailed summary has been reviewed recently[4,15] so here we only give a few basic steps. The starting point is the construction of a dynamical vector variable $\mathbf{A}_{\mathbf{q}}$, which consist of a relevant number of spin and quadrupolar operators. For $\mathbf{A}_{\mathbf{q}}$ the exact first- and second-order equations of motion can, by separating out all terms proportional to $\mathbf{A}_{\mathbf{q}}$, be written as (we set $\hbar=1$)

$$i\dot{\mathbf{A}}_{\mathbf{q}}=[\mathbf{A}_{\mathbf{q}},\mathcal{H}]=\langle\underline{\omega}_{\mathbf{q}}\rangle\mathbf{A}_{\mathbf{q}}+\mathbf{X}_{\mathbf{q}}\ , \tag{4}$$

$$-\ddot{\mathbf{A}}_{\mathbf{q}}=\langle\underline{\omega}_{\mathbf{q}}^2\rangle\mathbf{A}_{\mathbf{q}}+X_{\mathbf{q}}^{(2)}\ , \tag{5}$$

$$\underline{\Delta}_{\mathbf{q}}^2=\langle\underline{\omega}_{\mathbf{q}}^2\rangle-\langle\underline{\omega}_{\mathbf{q}}\rangle^2\ . \tag{6}$$

$\mathbf{X}_{\mathbf{q}}$ and $\mathbf{X}_{\mathbf{q}}^{(2)}$ are the so-called random forces which are not proportional to $\mathbf{A}_{\mathbf{q}}$. $\langle\underline{\omega}_{\mathbf{q}}^n\rangle$ is the frequency moment matrices of the relaxation function $(\mathbf{A}_{\mathbf{q}}\mathbf{A}_{\mathbf{q}}^\dagger)_\omega$. If $\underline{\Delta}_{\mathbf{q}}^2$ is nonzero, it directly tells us that the spectrum does not consist of δ functions, but that the excitations have a finite line width. Using $i(\dot{\mathbf{A}}\mathbf{B}^\dagger)=\langle[\mathbf{A},\mathbf{B}^\dagger]\rangle$ we can derive exact matrix equations for the first moment and the susceptibility matrices

$$\underline{\chi}_{\mathbf{q}}=\langle\underline{\omega}_{\mathbf{q}}\rangle^{-1}\mathbf{I},\quad \langle\underline{\omega}_{\mathbf{q}}\rangle=\mathbf{I}\underline{\chi}_{\mathbf{q}}^{-1}\ , \tag{7}$$

$$\mathbf{I}=\langle[\mathbf{A}_{\mathbf{q}},\mathbf{A}_{\mathbf{q}}^\dagger]\rangle\ . \tag{8}$$

Similarly using (5) we can deduce the following expressions which explicitly include correlation effects:

$$\langle\underline{\omega}_{\mathbf{q}}\rangle=\mathbf{I}(\langle\underline{\omega}_{\mathbf{q}}\rangle\mathbf{I}+\underline{\rho}_{\mathbf{q}})^{-1}(\langle\underline{\omega}_{\mathbf{q}}\rangle^2+\underline{\Delta}_{\mathbf{q}}^2)=\mathbf{I}\underline{\rho}_{\mathbf{q}}^{-1}\langle\underline{\omega}_{\mathbf{q}}\rangle^2\ , \tag{9}$$

$$\underline{\chi}_{\mathbf{q}}=(\langle\underline{\omega}_{\mathbf{q}}\rangle^2+\underline{\Delta}_{\mathbf{q}}^2)^{-1}(\langle\underline{\omega}_{\mathbf{q}}\rangle\mathbf{I}+\underline{\rho}_{\mathbf{q}})=\underline{\Delta}_{\mathbf{q}}^{-2}\underline{\rho}_{\mathbf{q}}\ , \tag{10}$$

$$\underline{\rho}_{\mathbf{q}}=\langle[\mathbf{X}_{\mathbf{q}},\mathbf{A}_{\mathbf{q}}^\dagger]\rangle\ . \tag{11}$$

The reason why it is advantageous to use the second-order time derivative to define the first moment and susceptibility is, that this includes the time-dependent varia-

tions in the neighborhood of the operator we are dealing with. Therefore, the correlation with the neighborhood is explicitly involved. The relations (9) and (10) constitute a useful starting point for approximations as well as the following exact formal solution by Mori[16] for the frequency dependence of the Laplace transformed dynamical relaxation function

$$(\mathbf{A}_q \mathbf{A}_q^\dagger)_z = \underline{\chi}_q [z\mathbf{I} - i\langle \underline{\omega}_q \rangle + \underline{\Sigma}_q(z)]^{-1} ,$$
$$\underline{\Sigma}_q(z) = (\mathbf{X}_q \mathbf{X}_q^\dagger)_z \underline{\chi}_q^{-1} . \tag{12}$$

A number of exact results for the formal theory are summarized in Ref. 4. The approximation made in the correlation theory consists of the following three assumptions: (a) that the effect of the remaining operator $\mathbf{X}_q^{(2)}$ in (5) can be neglected, (b) that the terms in $\dot{\mathbf{A}}_q(4)$ proportional to $\mathbf{A}_q$ obtained by the random-phase-approximation (RPA) decoupling, and the terms in $\ddot{\mathbf{A}}_q$ (5) proportional to $\mathbf{A}_q$, obtained by a mode-mode decoupling of all triple products of operators such as

$$ABC \sim \langle AB \rangle C + \langle AC \rangle B + \langle BC \rangle A ,$$

are sufficiently close to the exact projections so we can use the Mori result (12), and finally (c) the dynamical assumption that the second-order random-phase relaxation function is unimportant in the frequency range of interest. In the following we will apply the general theory to two specific cases. The task is to identify the relevant dynamical variables $\mathbf{A}_q$, to perform the commutators Eqs. (4) and (5), perform the decouplings and then perform the self-consistent numerical evaluation of thermodynamic quantities.

B. Magnetic excitations when the external magnetic field is parallel to the z axis

The induced magnetization and the internal field are for the field along the z axis given by

$$M_1 = \langle S_0^z \rangle , \quad H_1 = H_\parallel + J_0^\parallel M_1 . \tag{13}$$

Here H_1 is the molecular field and M_1 the induced magnetization along the field. For the transverse excitations corresponding to S_q^x and S_q^y modes, we need the dynamical variable vector

$$\mathbf{A}_q = \text{column}(S_q^x, L_q^y, S_q^y, L_q^x) . \tag{14}$$

The L_q^α operators are generated by the equations of motion for S_q^α. The first-moment matrix is directly found from (4) by a RPA decoupling of operators on different sites, as for example

$$\sum_k J_{k+q}^\parallel S_{k+q}^y S_{-k}^z \sim J_q^\parallel \langle S_0^z \rangle S_q^y .$$

Operators on the same site are treated exactly,

$$\langle \underline{\omega}_q \rangle = \frac{(\dot{\mathbf{A}}_q \mathbf{A}_q^\dagger)}{(\mathbf{A}_q \mathbf{A}_q^\dagger)} = i \begin{bmatrix} 0 & 0 & H_q^y & -D \\ 0 & 0 & -D_q^y & H_1 \\ -H_q^x & D & 0 & 0 \\ D_q^x & -H_1 & 0 & 0 \end{bmatrix} . \tag{15}$$

We introduce the $\mathbf{q}$-dependent field and anisotropy terms

$$H_q^\alpha = H_1 - J_q^\perp M_1 , \quad D_q^\alpha = D - J_q^\perp Q^\alpha , \tag{16}$$

and the squared frequencies

$$\omega_{qex}^2 = H_q^x H_q^y , \quad \omega_{qD}^{\alpha 2} = D D_q^\alpha , \tag{17}$$

where $Q^\alpha = \langle \hat{Q}_\alpha \rangle$, $\alpha = x,y$, and by symmetry $Q^x = Q^y$. Here ω_{qex} is the frequency found in the absence of the anisotropy D, and ω_{qD}^α is the exciton frequency found in the absence of magnetic order.

The eigenvalues $\lambda_{q\pm}$ for (15) are the solutions of the determinant equation. Then the dispersion relation for the Hamiltonian (2) can be written

$$\lambda_{q\pm}^2 = \tfrac{1}{2}\Omega_1^2 [1 \pm (1 - 4\omega_{q1}^2/\Omega_1^2)^{1/2}] ,$$
$$\Omega_1^2 = \omega_{qD}^{y2} + \omega_{qD}^2 + \omega_{qex}^2 + H_1^2 , \tag{18a}$$
$$\omega_{q1} = (H_1 H_q^\alpha - \omega_{qD}^{\alpha 2})/\Omega_1 .$$

If we neglect the transverse part of (18a), i.e., all $J_q^\perp$ terms, we get the mean-field result $\lambda_{q\pm}^2 = (D \pm H_1)^2$. This shows that the degenerate crystal-field doublet at D is split up in two modes by the internal field H_1. The eigenvalue λ_{q+} belongs to resonance frequencies from the ground state to the upper excited mode. The other eigenvalue λ_{q-} corresponds to excitations between the ground state and the first excited state. Without writing the full derivation for the effect of including the dipole forces we give the dispersion relation for the modes which are nondegenerate in their presence as the solution to the following equation:[15]

$$(\omega^2 - \lambda_{q+}^2)(\omega^2 - \lambda_{q-}^2) = |2K_q|^2 \{(H_1 M_1 - D Q^\alpha)^2 - \omega^2 M_1^2\} . \tag{18b}$$

The solutions of (18b) gives the dispersion relation for the full Hamiltonian (1). In order to derive the susceptibility matrix $\underline{\chi}_q$ from (7) we have to determine the matrix $\mathbf{I}$ which can be directly found from (8)

$$\mathbf{I} = \langle [\mathbf{A}_q \mathbf{A}_q^\dagger] \rangle = i \begin{bmatrix} 0 & 0 & M_1 & -Q^x \\ 0 & 0 & -Q^y & M_1 \\ -M_1 & Q^y & 0 & 0 \\ Q^x & -M_1 & 0 & 0 \end{bmatrix} ,$$
$$\underline{\chi}_q = \langle \underline{\omega}_q \rangle^{-1} \mathbf{I} . \tag{19}$$

The RPA susceptibility for the transverse modes are found by using the (1,1) and (3,3) matrix elements of (19):

$$\chi_q^\alpha = (S_q^\alpha S_q^{\alpha\dagger}) = \frac{1}{R_1^\alpha - J_q^\perp} , \tag{20}$$

where R_1^α is the inverse local susceptibility which is found to be

$$R_1^\alpha = \frac{1}{\chi_0^{\alpha\alpha}} = \frac{H_1^2 - D^2}{H_1 M_1 - D Q^\alpha} . \tag{21}$$

If M_1 and Q^α are evaluated in the mean-field approximation, (21) agrees exactly with the directly calculated Van

Vleck susceptibility.[17] This shows that the decoupling is exact with respect to single-site properties. Using (17) and (20) we can derive the following simpler expression for the lowest excitation frequency. When this is much smaller than the upper mode frequency we can expand $\lambda_{q-}^2 \approx \omega_{q1}^2$ and rewrite this as

$$\omega_{q1} = K_1 M_1 / \chi_q^\alpha , \tag{22}$$

K_1 is a weakly $\mathbf{q}$-dependent constant of order 1. Equation (22) shows that the first-moment frequency vanishes at the temperature or magnetic field at which χ_q^α diverges for a special $\mathbf{q}$. As can be seen from Eq. (7), this is an exact result if the exact first moment is known. The RPA expression for this is quite accurate, provided that the involved thermodynamic averages are calculated self-consistently, including the $\mathbf{q}$-dependent dispersion and using sums over $\mathbf{q}$. This level of sophistication is closely related to the so-called spherical approximation for a Heisenberg magnet. With this one can predict the transition temperature correctly within a few percent.[8]

C. Magnetic excitations when the external magnetic field is perpendicular to the z axis

The induced magnetization and the molecular field are for the field along the x axis, perpendicular to the z axis defined as

$$M_2 = \langle S_0^x \rangle , \quad H_2 = H_\perp + J_0^\perp M_2 . \tag{23}$$

Here H_2 is the internal field and M_2 the induced magnetization along it. We need now the dynamical variable vector

$$\mathbf{A}_q = \text{column}(S_q^y, L_q^z, S_q^z, L_q^y) . \tag{24}$$

For the first-moment frequency matrix we obtain

$$\langle \underline{\omega}_q \rangle = i \begin{bmatrix} 0 & 0 & H_q^z & D \\ 0 & 0 & -D_q^z & H_2 \\ -H_q^y & 0 & 0 & 0 \\ D_q^y & -H_2 & 0 & 0 \end{bmatrix} , \tag{25}$$

which we have defined with the same notations as in (16), but in addition we have introduced

$$H_q^y = H_2 - J_q^\perp M_2 , \quad H_q^z = H_2 - J_q^\parallel M_2 \tag{26}$$

and

$$D_q^z = -J_q^\parallel Q^z , \quad Q^z = \langle \hat{Q}_z \rangle . \tag{27}$$

We introduce the following squared frequencies:

$$\omega_{qex}^2 = H_q^y H_q^z , \quad \omega_{qD}^2 = D D_q^z , \tag{28}$$

where ω_{qex} is the frequency in absence of anisotropy and ω_{qD}^x that in absence of the external field. The eigenvalues $\lambda_{q\pm}$ for the Hamiltonian (2) are the solutions of the determinant equation (25)

$$\begin{aligned} \lambda_{q\pm}^2 &= \tfrac{1}{2}\Omega_2^2 [1 \pm (1 - 4\omega_{q2}^2/\Omega_2^2)^{1/2}] , \\ \Omega_2^2 &= \omega_{qD}^{z2} + \omega_{qex}^2 + H_2^2 , \\ \omega_{q2}^2 &= H_2 H_q^y (H_2 H_q^z - \omega_{qD}^{z2})/\Omega_2^2 . \end{aligned} \tag{29}$$

If we are neglecting all exchange interactions, i.e., $J_q^\perp = J_q^\parallel = 0$, we reduce our Hamiltonian to a simple localized one. Accordingly we get the mean-field eigenvalues $\lambda_{q\pm} = \frac{1}{2}[D \pm (D^2 + 4H_\perp^2)^{1/2}]$. This shows that, contrary to the case $H \parallel z$ axis, one mode of the doublet moves to higher energies, while the ground state lowers its energy with increasing field.

The matrix $\mathbf{I}$ and the susceptibility matrix $\underline{\chi}_q$ in (7) are

$$\mathbf{I} = i \begin{bmatrix} 0 & 0 & M_2 & Q^y \\ 0 & 0 & Q^z & M_2 \\ -M_2 & -Q^z & 0 & 0 \\ -Q^y & -M_2 & 0 & 0 \end{bmatrix} , \quad \underline{\chi}_q = \langle \underline{\omega}_q \rangle^{-1} \mathbf{I} . \tag{30}$$

The RPA susceptibilities are given by the (1,1) and (3,3) matrix elements and read

$$\begin{aligned} \chi_{q2}^y &= (S_q^y S_{-q}^y) = \frac{1}{R_2^y - J_q^\perp} , \\ \chi_{q2}^z &= (S_q^z S_{-q}^z) = \frac{1}{R_2^z - J_q^\parallel} , \end{aligned} \tag{31}$$

where the local inverse susceptibilities are

$$R_2^y = \frac{1}{\chi_0^{yy}} = \frac{H_2}{M_2} , \tag{32}$$

$$R_2^z = \frac{1}{\chi_0^{zz}} = \frac{H_2}{H_2 M_2 - D Q^z} . \tag{33}$$

Similarly to (22), λ_{q-} can be reformulated in terms of the susceptibilities (31)

$$\lambda_{q-} \approx \omega_{q2} = K_2 M_2 / (\chi_{q2}^y \chi_{q2}^z)^{1/2} , \tag{34}$$

where K_2 is of order 1. This shows that the first moment vanishes, although differently from the previous case, when the critical susceptibility component χ_{q2}^y diverges.

D. Inclusion of fluctuation effects

In order to clarify the discussion the dipole forces are neglected in the following. We use the result (9) to calculate the fluctuation effects by decoupling the second-order equation of motion for the dynamical spin variables. For both cases—the external magnetic field parallel and perpendicular to the z axis—we find that the $\underline{\rho}_q$ and $\underline{\Delta}_q$ matrices are diagonal. The matrix elements for the spin operators are given by the expressions

$$\rho_q = C_q^{(1)} , \quad \Delta_q^2 = C_q^{(2)} - C_q^{(1)} \mathbf{J}_q , \quad \chi_q = \rho_q / \Delta_q^2 , \tag{35}$$

where $C_q^{(1)}$ and $C_q^{(2)}$ are correlation functions in various combinations. Calculating the susceptibility according to (10) one finds that the general RPA form of the susceptibility is recovered but that the local susceptibilities

$1/R^{\alpha}$ are replaced by renormalized and, in principle, wave-vector-dependent susceptibilities $1/R^{\alpha}_{\mathbf{q}}$. For case (1), where the magnetic field is parallel to the z axis, we find that R^{x}_{1} must be replaced by

$$R^{x}_{1}\rightarrow R^{x}_{\mathbf{q}1}=C^{x(2)}_{\mathbf{q}}/C^{x(1)}_{\mathbf{q}}\ ,$$
$$C^{x(n)}_{\mathbf{q}}=\frac{1}{N}\sum_{\mathbf{k}}\Big[(J_{\mathbf{k}}-J_{\mathbf{k}-\mathbf{q}})J^{(n-1)}_{\mathbf{k}}\langle\delta S^{z}_{\mathbf{k}}\delta S^{z}_{-\mathbf{k}}\rangle + (J_{\mathbf{k}}-J_{\mathbf{k}-\mathbf{q}})J^{(n-1)}_{\mathbf{k}}\langle S^{y}_{\mathbf{k}}S^{y}_{-\mathbf{k}}\rangle\Big]\ , \tag{36}$$

where $\delta S^{z}_{\mathbf{k}}=S^{z}_{\mathbf{k}}-\langle S^{z}_{0}\rangle$ and $J^{(n-1)}_{\mathbf{k}}$ is 1 and $J_{\mathbf{k}}$ for $n=1$ and 2, respectively. By symmetry, $R^{x}_{\mathbf{q}1}=R^{y}_{\mathbf{q}1}$. At low temperatures the longitudinal (z) fluctuations can be neglected. Since $(1/NJ_0)\sum_{\mathbf{k}}J_{\mathbf{k}}\langle S^{\alpha}_{\mathbf{k}}S^{\alpha}_{-\mathbf{k}}\rangle$ is a nearest-neighbor correlation function and $(1/NJ^{2}_{0})\sum_{\mathbf{k}}J^{2}_{\mathbf{k}}\langle S^{\alpha}_{\mathbf{k}}S^{\alpha}_{-\mathbf{k}}\rangle$ is a sum of an on-site and a next-nearest-neighbor correlation function, $R^{x}_{\mathbf{q}1}$ is a nonlocal inverse susceptibility for a small cluster.

In case (2), where the magnetic field is perpendicular to the z axis, we find that R^{α}_{2} must be replaced by

$$R^{y}_{2}\rightarrow R^{y}_{\mathbf{q}2}=C^{y(2)}_{\mathbf{q}}/C^{y(1)}_{\mathbf{q}},\quad R^{z}_{2}\rightarrow R^{z}_{\mathbf{q}2}=C^{z(2)}_{\mathbf{q}}/C^{z(1)}_{\mathbf{q}}\ , \tag{37}$$

where the $C^{\alpha(n)}_{\mathbf{q}}$ are obtained from (36) by cyclic permutations and now $\delta S^{x}_{\mathbf{k}}$ is inserted instead of $S^{x}_{\mathbf{k}}$. However, these longitudinal terms can be neglected at low temperatures.

IV. NUMERICAL CALCULATION OF THE SOFT MODE AND OF INCOMMENSURATE ORDERING

The possibility of inducing a phase transition in $CsFeCl_3$ and $CsFeBr_3$ to three-dimensional magnetic ordering by applying an external magnetic field along the z direction have stimulated many physicists to investigate the behavior of the excitation spectrum and the nature of the phase transition.[12,18,19] A recent detailed experimental study of $CsFeBr_3$ has shown that the field-induced phase transition can be classified to be of second order.[19] In the following we show that a fully self-consistent RPA can well reproduce the excitation spectrum below the phase transition. It seems to fail to describe accurately the region of the phase transition. However, the calculated correlation functions, correlation lengths, and specific heat strongly indicate the approach of a phase transition of second order.

In $CsFeCl_3$ an onset of incommensurate ordering has been detected experimentally as a function of the applied magnetic field.[12] The inclusion of fluctuation effects can explain this field-induced incommensurability.[15]

A. Self-consistent RPA Theory

Let us consider the case where the field is along the z direction. In order to obtain the excitation frequencies at finite temperatures and fields we have to calculate self-consistently the thermodynamic quantities, the average quadrupole moment $Q^{\alpha}=-Q$, and the induced magnetization M_1. Using $S(S+1)=2=S^{2}_{x}+S^{2}_{y}+S^{2}_{z}$ we can write

$$(\hat{Q}_x+\hat{Q}_y)/2=2S(S+1)-3(S^{2}_{x}+S^{2}_{y})$$

or by using the symmetry,[5] write

$$Q=-4+\frac{3}{2N}\sum_{\mathbf{q}}\langle S^{+}_{\mathbf{q}}S^{-}_{-\mathbf{q}}+S^{-}_{\mathbf{q}}S^{+}_{-\mathbf{q}}\rangle\ . \tag{38}$$

The spin-correlation function $\langle S^{+}_{\mathbf{q}}S^{-}_{-\mathbf{q}}\rangle$ can be determined from the imaginary part of dynamical susceptibility according to the dissipation fluctuation theorem. This is simply related to the relaxation function we have introduced in Sec. III A:

$$\mathrm{Im}\chi^{+-}(\mathbf{q},\omega)=\omega\,\mathrm{Re}(S^{+}_{\mathbf{q}}S^{-}_{-\mathbf{q}})_{z=i\omega+\epsilon\rightarrow 0}\ .$$

If we neglect line-shape effects the general result is given in Eq. (12) for $\underline{\Sigma}_{\mathbf{q}}(z)=0$ in terms of the eigenvalues for the first moment $\langle\underline{\omega}_{\mathbf{q}}\rangle$, in Eqs. (18a) and (18b)

$$\langle S^{+}_{\mathbf{q}}S^{-}_{-\mathbf{q}}\rangle=\int\frac{d\omega}{\pi}\frac{\omega\,\mathrm{Re}(S^{+}_{\mathbf{q}}S^{-}_{-\mathbf{q}})_{z=i\omega}}{1-\exp(-\beta\omega)}\ , \tag{39}$$

and similarly for $(-+)$. Finally we get the following two equations for the Q factor and the induced magnetization M_1

$$Q=\frac{-4+(3/2N)\sum_{\mathbf{q}}\{[M_1(J_{\mathbf{q}}M_1+\lambda^{0}_{\mathbf{q}})](\lambda^{0}_{\mathbf{q}})^{-1}[\coth(\Omega^{-}_{\mathbf{q}})-\coth(\Omega^{+}_{\mathbf{q}})]+2M_1\coth(\Omega^{+}_{\mathbf{q}})\}}{1+(3/2N)\sum_{\mathbf{q}}D(\lambda^{0}_{\mathbf{q}})^{-1}[\coth(\Omega^{-}_{\mathbf{q}})-\coth(\Omega^{+}_{\mathbf{q}})]} \tag{40}$$

where $\Omega^{\pm}_{\mathbf{q}}=\frac{1}{2}\beta\lambda_{\mathbf{q}\pm}$, $\lambda^{0}_{\mathbf{q}}=\frac{1}{2}(\lambda_{\mathbf{q}+}+\lambda_{\mathbf{q}-})$ in terms of the solutions (18a). By introducing the standard basis operators $\hat{a}_{pn}=|p\rangle\langle n|$ and solving the equations of motion, Hayley and Erdös[3] introduce a monotopic condition which leads to the same expression for the Q factor. They also give the following expression for the induced moment

$$M_1=\frac{4(1+X)}{1+3(1+X)^2+(2-3Y)Y}\ , \tag{41}$$

where

$$X=-1+\frac{1}{N}\sum_{\mathbf{q}}\frac{\sinh(\beta\tilde{\lambda}_{\mathbf{q}})+J_{\mathbf{q}}M_1(2\lambda^{0}_{\mathbf{q}})^{-1}\sinh(\beta\lambda^{0}_{\mathbf{q}})}{\cosh(\beta\tilde{\lambda}_{\mathbf{q}})-\cosh(\beta\lambda^{0}_{\mathbf{q}})}\ ,$$
$$Y=-\frac{D}{N}\sum_{\mathbf{q}}\frac{(\lambda^{0}_{\mathbf{q}})^{-1}\sinh(\beta\lambda^{0}_{\mathbf{q}})}{\cosh(\beta\tilde{\lambda}_{\mathbf{q}})-\cosh(\beta\lambda^{0}_{\mathbf{q}})},\quad \tilde{\lambda}_{\mathbf{q}}=\tfrac{1}{2}(\lambda_{\mathbf{q}+}-\lambda_{\mathbf{q}-})\ .$$

With Eqs. (40) and (41) it is possible to determine the dispersion of the excitations as a function of temperature

and magnetic field numerically self-consistent. Figures 1(a), 1(b), and 1(c) show the results of a fully self-consistent RPA calculation for $CsFeBr_3$ and $CsFeCl_3$. We have calculated the excitation frequencies at the K point as a function of the magnetic field [Fig. 1(a)]. We see that for magnetic fields below the critical magnetic field the calculated excitation frequencies describe very well the measured ones. The calculated quadrupole moment Q [Fig. 1(b)] and the induced magnetization M_1 [Fig. 1(c)] are also shown. It would be of considerable interest as a check on the present theory if Q could be determined directly experimentally.

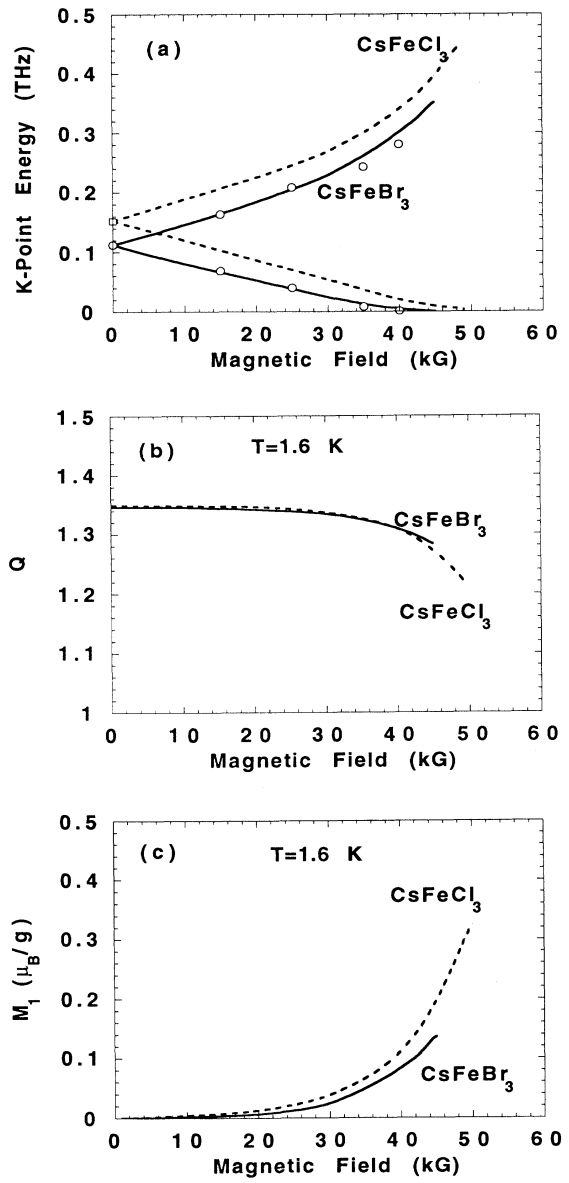

FIG. 1. (a) Calculated excitation frequencies for $CsFeBr_3$ (full line) and $CsFeCl_3$ (hatched line) at $T=1.6$ K as a function of the magnetic field parallel to the z axis. Experimental values (○) for $CsFeBr_3$ are from Ref. 18 and (□) for $CsFeCl_3$ (Ref. 20). (b) Calculated quadrupole moment Q for $CsFeBr_3$ (full line) and $CsFeCl_3$ (hatched line) at $T=1.6$ K as a function of the magnetic field parallel to the z axis. (c) Calculated induced magnetization M_1 for $CsFeBr_3$ (full line) and $CsFeCl_3$ (hatched line) at $T=1.6$ K as a function of the magnetic field parallel to the z axis.

The used anisotropy and exchange parameters have been determined by fitting (18a) to the measured excitations at zero field.[14,20] In Table I we have listed the obtained parameters. The $g_{\parallel}$ factor used in our calculation has been determined experimentally as $g_{\parallel}\sim 2.4$ for both $CsFeBr_3$ and $CsFeCl_3$.[12,18] We calculate for the critical field in $CsFeBr_3$, $H_c\approx 45$ kG and in $CsFeCl_3$, $H_c\approx 50$ kG.

It has to be pointed out that a numerical self-consistent solution of (40) and (41) using an iteration method is only possible for fields below 37 kG in $CsFeBr_3$ and below 39 kG in $CsFeCl_3$. In the following we discuss a semigraphical and seminumerical method we have developed to get self-consistent results for the induced magnetization and the quadrupole moment beyond these magnetic fields. We use the results on $CsFeBr_3$ as an example. At higher magnetic fields than 37 kG in $CsFeBr_3$ the calculated frequencies in the $\mathbf{q}$ space in the neighborhood of the K point may become negative because the soft mode is approaching the frequency zero with increasing magnetic field and a small deviation of the chosen start parameters Q and M_1 from the real solution has a large influence on the calculated frequencies around the K point. To obtain high accuracy in the $\mathbf{q}$ summations we have divided the hexagonal Brillouin zone along the directions Γ-M and M-K as well as perpendicular to these directions in 61 points each. In a second step the eight nearest boxes to the K point are further subdivided into 64 boxes each. To get a self-consistent solution for Q and M_1 for $H>37$ kG, we used the graphical procedure the results of which are shown in Fig. 2. This is done as follows. For a fixed magnetic field the quadrupole moment $Q_{\rm calc}$ is calculated for a fixed magnetization $M_{1\rm fix}$ and for different start parameters $Q_{\rm start}$. We use (40) by calculating for each box of the $\mathbf{q}$ space the two excitation frequencies. If at least one of the calculated frequencies is negative we draw the conclusion that $Q_{\rm calc}$ does not exist for the chosen set of the starting parameters. Finally, we determine graphically the solution of the following equation:

$$Q_{\rm calc}(Q_{\rm start},M_{1\rm fix})=Q_{\rm start}\ . \tag{42}$$

We repeat this calculation for another fixed magnetization $M_{1\rm fix}$. At the end we get for different values of the fixed magnetization $M_{1\rm fix}$ self-consistently determined values for the quadrupole moment $Q_{\rm calc}$. In a second step

TABLE I. The parameter sets in THz used for $CsFeBr_3$ (from Ref. 14) and $CsFeCl_3$ (from Ref. 20). D denotes the ion anisotropy, J_1 and J_2 are exchange parameters between nearest and next-nearest neighbors along the z direction, J' is the exchange parameter between nearest neighbors in the hexagonal plane.

	D	J_1	J_2	J'
$CsFeBr_3$	0.621	−0.066		−0.0062
$CsFeCl_3$	0.522	0.0629	−0.0095	−0.0042

we calculate in a similar way self-consistently determined values for the magnetization $M_{1\text{calc}}$ by using (41) as a function of fixed values for the quadrupole moment Q_{fix}, i.e., we determine the solutions of the equation

$$M_{\text{calc}}(M_{\text{start}},Q_{\text{fix}})=M_{\text{start}} \ . \tag{43}$$

The graphical determined solutions of (42) and (43) are shown in Fig. 2 for various magnetic fields. The intersecting point of the two functions (42) and (43) determines the required self-consistent solutions. For magnetic fields $H^{\text{ext}}\geq 46$ kG, no graphical solution is found. We interpret this feature as the onset of the three-dimensional magnetic ordering: A more elaborate theory is needed for describing the ordered phase with the same degree of accuracy, including up to seven self-consistent parameters.

We obtain for the critical field $H_c\sim 45$ kG. In recent experiments on $CsFeBr_3$ we have determined a critical magnetic field of $H_c=40.2\pm 0.5$ kG.[19] The difference between the RPA results, which are self-consistent in the "spherical" approximation, and the experimental value is related to neglecting the explicit nearest-neighbor correlation functions. The critical field is slightly overestimated ($\approx 10\%$) by the RPA theory and the softening of the first moment is underestimated. The RPA theory is an excellent description of the experimental data far below the critical magnetic field. For magnetic fields which are comparable to the critical field the RPA results can only be qualitatively interpreted.

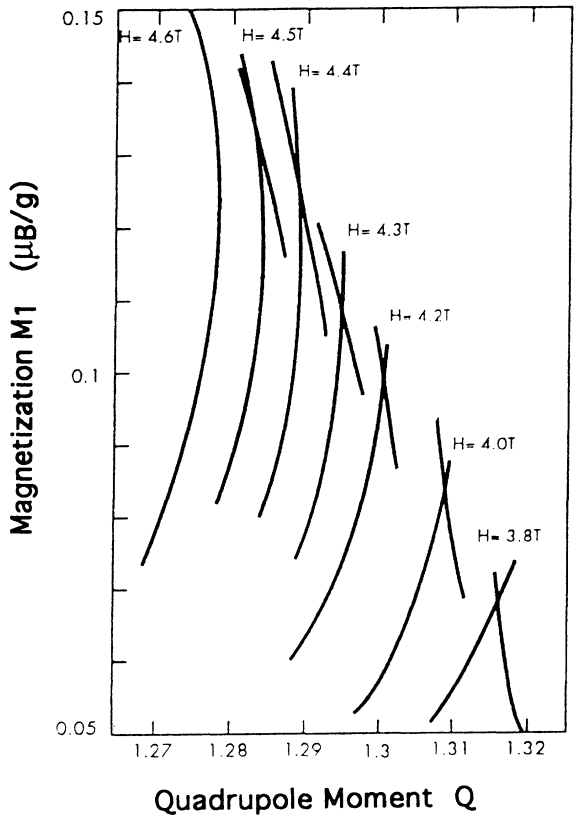

FIG. 2. Graphical, self-consistent determined solution for the quadrupole moment Q and the induced magnetization M_1 for magnetic fields $H\geq 38$ kG. The upwards sloping curves are the self-consistently calculated $Q(M)$ for various M from (42); and the crossing curves are $M(Q)$ from (43) for various Q. Where the curves cross the fully self-consistent solution is found. There is no solution for $H=4.6$ T$=46$ kG.

The free energy F is given by the following exact relation:[4,21]

$$F=\langle\mathcal{H}\rangle_{T=0}-T\int_0^T(\langle\mathcal{H}\rangle_{T'}-\langle\mathcal{H}\rangle_{T=0})\frac{dT'}{T'^2} \ . \tag{44}$$

In this equation, the self-consistently calculated functions entering in $\langle\mathcal{H}\rangle$ from (1) should be inserted. Integrating (44) yields for the δ-function response in the RPA theory the harmonic oscillator result[22] for the free energy and the specific heat

$$\begin{aligned} F&=F_{T=0}+k_BT\sum_{qp}\ln[1-\exp(-\beta\lambda_{qp})] \ , \\ C_V&=\sum_{qp}(\beta\lambda_{qp})^2\exp\beta\lambda_{qp}/(\exp\beta\lambda_{qp}-1)^2 \ , \end{aligned} \tag{45}$$

where $F_{T=0}$ denotes the quantum-mechanical zero-point energy and λ_{qp} denotes the eigenvalue ($p=\pm$). In Fig. 3(a) we have shown the calculated free energy as a function of the magnetic field (for clarity we have set $F_{T=0}=0$), and Fig. 3(b) shows the corresponding specific

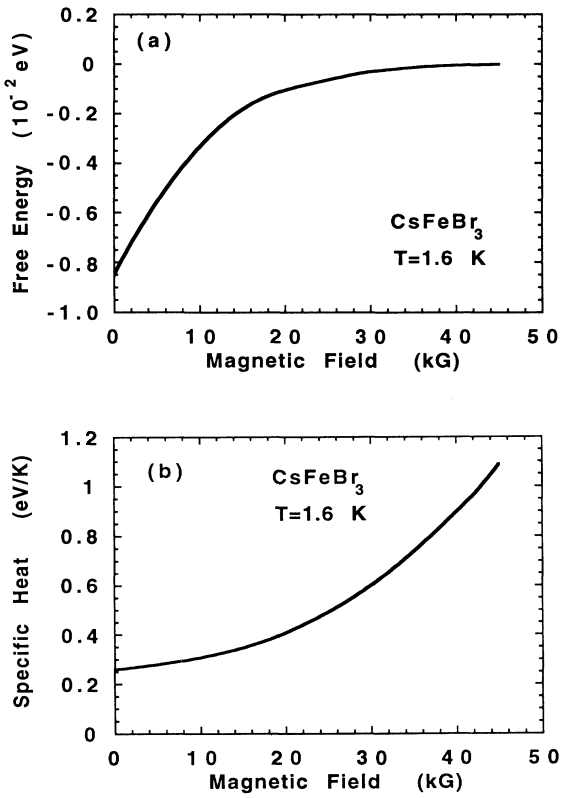

FIG. 3. (a) Calculation of the free energy as a function of the magnetic field according to Eq. (45). For clarity we have set $E_{T=0}=0$. (b) Specific heat as a function of the magnetic field according to (45).

heat. The latter is strongly increasing for $H \rightarrow H_c$ indicating the approach to a second-order phase transition. Figure 4 shows the calculated correlation function for $\mathbf{q}$ along Γ-K $\langle S^x_{\mathbf{q}} S^x_{-\mathbf{q}} \rangle$ as a function of the magnetic field. This is proportional to the integrated inelastic-scattering intensity, which can be determined by neutron scattering. Near $\mathbf{q}=\mathbf{Q}_{K \text{ point}}$ the correlation function is found to be of the expected Lorentzian form

$$\langle S^x_{\mathbf{q}} S^x_{-\mathbf{q}} \rangle = \frac{C}{\xi_x^{-2}+q^2} , \tag{46}$$

where C is a constant and $\mathbf{Q}-\mathbf{Q}_{K \text{ point}}=\mathbf{q}$. Correlation lengths deduced from (46) are shown in Fig. 5 for different field values. The strong increase in the calculated critical peak intensity and in the deduced correlation lengths at the K point for $H \rightarrow H_c$ further supports that the transition is approaching a second-order phase transition. These results are based on the analysis of the self-consistently calculated first-moment frequency. The actual line shape for the excitations for fields close to H_c is expected to broaden and become overdamped at least for $\mathbf{q}$ close to the critical $\mathbf{q}$ vector $\mathbf{Q}_{K \text{ point}}$.

B. Field-induced incommensurability and fluctuation effects

The influence of the dipolar forces may be neglected for explaining the occurrence of incommensurability because the excited modes are, according to Eq. (18b), already split by the magnetic field along the z direction, as argued in Ref. 15. It has been checked that when including the dipole terms Eq. (1), the minimum in the RPA-dispersion relation remains at the K point for fields $H \approx H_c$. The details in the selection of $\mathbf{q}$ vectors at the field-induced incommensurability found for $CsFeCl_3$ are a result of an interplay between the large correlation effects due to the low dimensionality of this system and the dipolar effects.

Because several of the dynamical variables in (14) do not couple when the magnetic field is applied parallel to the z axis we need to consider only two operators in our dynamical vector $\mathbf{A}_{\mathbf{q}}=(S^+_{\mathbf{q}}, L^-_{\mathbf{q}})$, where L^- is given by $S_z S^- + S^- S_z$, where $S^{\pm}=S^x \pm iS^y$. To determine the first-moment frequency matrix including fluctuation effects we have to evaluate (9). The dynamical variables generate the matrices

$$\mathbf{I}=2\begin{bmatrix} M_1 & Q \\ Q & M_1 \end{bmatrix}, \quad \langle \underline{\omega}_{\mathbf{q}} \rangle = \begin{bmatrix} H_1 - J_{\mathbf{q}} M_1 & D \\ D - J_{\mathbf{q}} Q & H_1 \end{bmatrix} , \tag{47}$$

$$\underline{\rho}_{\mathbf{q}} = \begin{bmatrix} (J_0 - J_{\mathbf{q}})(c_\perp^{(1)} + c_\parallel^{(1)}) & (J_0 - J_{\mathbf{q}}) m^{(1)} \\ (J_0 - J_{\mathbf{q}}) m^{(1)} & J_0(5c_\perp^{(1)} + c_\parallel^{(1)}) - J_{\mathbf{q}} s_\perp^{(1)} \end{bmatrix} , \tag{48}$$

$$\underline{\Delta}^2_{\mathbf{q}} = \frac{1}{2}\begin{bmatrix} (J_0 - J_{\mathbf{q}})[J_0(c_\perp^{(2)} + c_\parallel^{(2)}) - J_{\mathbf{q}}(c_\perp^{(1)} + c_\parallel^{(1)})] & 0 \\ -(J_0 - J_{\mathbf{q}}) J_{\mathbf{q}} m^{(1)} - J_0 J_{\mathbf{q}} m^{(2)} & J_0^2(5c_\perp^{(2)} + c_\parallel^{(2)}) \end{bmatrix} , \tag{49}$$

where in terms of $\gamma_{\mathbf{q}}=J_{\mathbf{q}}/J_0$

$$c_\perp^{(n)} = \frac{1}{N}\sum_{\mathbf{k}} \gamma_{\mathbf{k}}^n \langle S^+_{\mathbf{k}} S^-_{-\mathbf{k}} \rangle$$

and

$$c_\parallel^{(n)} = \frac{2}{N}\sum_{\mathbf{k}} \gamma_{\mathbf{k}}^n \langle \delta S^z_{\mathbf{k}} \delta S^z_{-\mathbf{k}} \rangle, \quad n=1,2 , \tag{50a}$$

$$s_\perp^{(1)} = \frac{1}{N}\sum_{\mathbf{k}} \gamma_{\mathbf{k}} (\langle L^+_{\mathbf{k}} L^-_{-\mathbf{k}} \rangle + \langle \text{quad} \rangle) , \tag{50b}$$

$$m^{(n)} = \frac{1}{2N}\sum_{\mathbf{k}} \gamma_{\mathbf{k}}^n (\langle L^-_{\mathbf{k}} S^-_{-\mathbf{k}} \rangle + \langle S^-_{\mathbf{k}} L^-_{-\mathbf{k}} \rangle), \quad n=1,2 . \tag{50c}$$

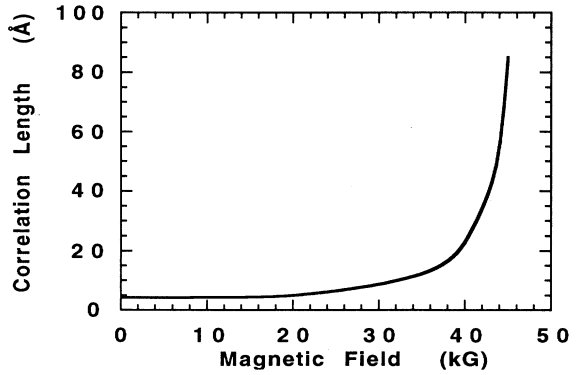

FIG. 4. Semilogarithmic plot of the correlation function $\langle S^x_{\mathbf{q}} S^x_{-\mathbf{q}} \rangle$ for $\mathbf{q}$ along the Γ-K direction as a function of the magnetic field. This contribution is proportional to the critical scattering which can be determined by neutron scattering.

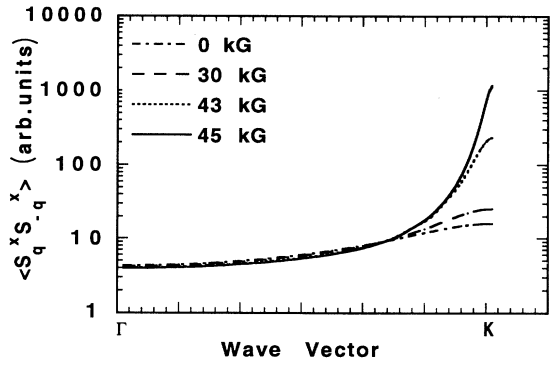

FIG. 5. Correlation lengths deduced from Eq. (46) as a function of the magnetic field.

Here $\langle \text{quad} \rangle$ stands for neglected correlations between longitudinal quadrupolar operators. The correlation functions $m^{(n)}$ are zero for $H=0$.

For $H=0$ the susceptibility (10) including correlation effects assumes the RPA functional form (20)

$$(S_q^+ S_{-q}^-)=\frac{2}{J_0}\frac{1}{R-\gamma_q}, \quad (L_q^+ L_{-q}^-)=\frac{2}{J_0 R'}, \qquad (51)$$

where $R=(c_\perp^{(2)}+c_\parallel^{(2)})/(c_\perp^{(1)}+c_\parallel^{(1)})$ and $R'\approx R$. R is the ratio of the correlation functions (50a) according to (35), (48), and (49), whereas $R_{\mathrm{RPA}}=D/J_0 Q$. The corresponding frequency is given by

$$\omega_q^2=J_0 Q D(R-\gamma_q),$$

which has the same form as $\omega_{qD}^{\alpha 2}$ in (17). When correlation effects are included, the RPA-functional form is correct for both the $\underline{\chi}_q$ and $\langle \underline{\omega}_q \rangle$ but the anisotropy constant D is replaced by $J_0 QR$. Therefore, D is also renormalized with temperature. In spite of strong renormalization of the RPA parameters in $CsFeCl_3$ at $H=0$ the minimum of the dispersion is still at the K point when dipolar forces are neglected. For finite magnetic fields R becomes $\mathbf{q}$ dependent, since the off-diagonal elements in (48) become finite. This yields the possibility of displacing the minimum ω_q from the K point. The excitation frequencies including correlation effects are given by the eigenvalues of (9) and therefore determined by (47)–(49). The RPA first-moment matrix $\langle \underline{\omega}_q \rangle$ has the eigenvalues $\lambda_{q\pm}$ of (18a). Magnetic ordering occurs when the minimum eigenvalue of (9) is approaching zero. To evaluate (9) we have first of all to determine the induced magnetization M_1 and the quadrupole moment Q. For our numerical calculations in $CsFeCl_3$ we used the same division in reciprocal space and the same semigraphical and seminumerical method for calculating M_1 and Q as described for $CsFeBr_3$. Figures 1(b) and 1(c) show the obtained results for Q and M_1. The parameters of the anisotropy and the exchange for $CsFeCl_3$ used in the calculations are summarized in Table I. We get a critical magnetic field of $H_c \sim 50$ kG for $T=1.6$ K.

For low magnetic fields the induced magnetization is small. The minimum of the energy still occurs at the K point as in the RPA theory when evaluating (9). For magnetic fields close to H_c the induced magnetic moment M_1 and also $m^{(1)}$ and $m^{(2)}$ are much larger in $CsFeCl_3$ than in $CsFeBr_3$ due to different interaction parameters. As a consequence, a minimum in the dispersion relation develops in a ring around the K point when evaluating (9). In our numerical calculations we have neglected the longitudinal correlation functions $c_\parallel^{(n)}$ and used only the in-plane exchange interaction when determining J_q and J_0 in (48) and (49). However, the full three-dimensional dispersion γ_q is used for evaluating the correlation functions (50). In Fig. 6 we show calculated transverse correlation functions (50) as a function of the magnetic field. The correlation functions $m^{(1)}$ and $m^{(2)}$, (50c), which determine the off-diagonal elements of (48) and (49) at magnetic fields near to the critical field $H_c=50$ kG, are sufficiently large to give rise to a displacement of the minimum of (9) from the K point. The numerical results are shown in Fig. 7 for $H=49$ kG indicating that a threefold symmetry around the K point should occur. This calculation shows that correlation effects alone can explain the onset of incommensurability in a field.

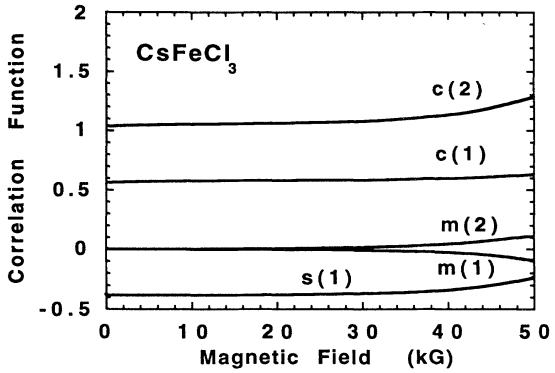

FIG. 6. Calculated transverse correlation functions for $CsFeCl_3$ according to Eqs. (50) as a function of the magnetic field parallel to the z axis.

Without dipolar forces the minimum at $H=49$ kG occurs at the wave vector $\mathbf{q}=(1,1/3-\epsilon,0)$, where $\epsilon=0.055$ and at the equivalent vectors [in reduced units in a rectangular coordinate system with $q_x^{\max}=q_z^{\max}=1$ and $q_y^{\max}=\frac{1}{3}$ and $q_{K\ \mathrm{point}}=(1,1/3,0)$]. The minimum is 2.1×10^{-5} THz below the K-point energy, which is given by 0.004 576 THz. The calculation thus gives a very flat dispersion in a region around the K point. In the present, more detailed calculation, the obtained wave-vector region in reciprocal space is in much better agreement with that found experimentally,[12] than that obtained in the

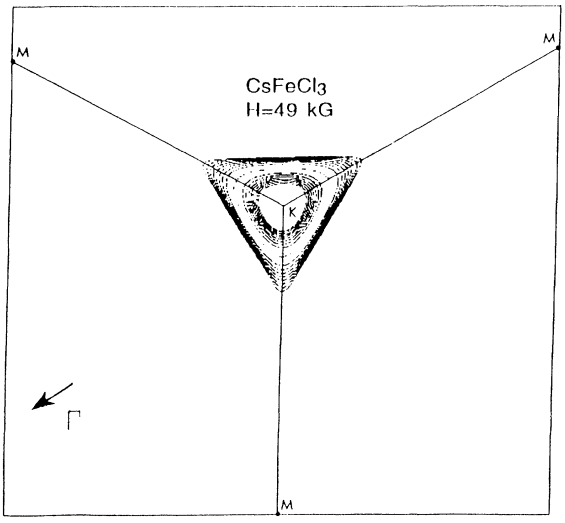

FIG. 7. Calculated excitation energies in $CsFeCl_3$ for $H=49$ kG parallel to the z axis including correlation effects. The minimum energy of the dispersion occurs in a ring around the K point yielding the possibility of the occurrence of incommensurable ordering. Dipole forces are neglected in these calculations.

preliminary calculation.[15] The interplay of correlation effects and dipolar forces may determine the exact position in reciprocal space where incommensurate ordering occurs.

In $CsFeBr_3$ the similar calculation of the frequencies (9) with the inclusion of correlation effects at $H=44$ kG gives no hints of a displacement of the energy minimum from the K point. Our numerical results show that the correlation functions $m^{(1)}$ and $m^{(2)}$ in $CsFeBr_3$ at 44 kG are only one-third of the value of the correlation functions $m^{(1)}$ and $m^{(2)}$ in $CsFeCl_3$ at 49 kG. The off-diagonal elements in (48) and (49) for $CsFeBr_3$ are not large enough to cause a displacement of the energy minimum from the K point. This is in agreement with the experimental observation of absence of incommensurability in $CsFeBr_3$.

V. CONCLUSION

In this work we have provided a theoretical description for the static and dynamic properties of the singlet-ground-state magnets on the basis of the correlation theory. This theory generalizes the RPA theory by including correlation effects which may become very important in low-dimensional magnets. As a starting point we deduced within the framework of CT mathematical expressions in the RPA for the dispersion relations in the presence of an external field. In a second step we included correlation effects and showed that the general RPA-functional expressions are recovered but that the local susceptibilities are replaced by renormalized and wave-vector-dependent ones. A numerical self-consistent RPA calculation yields critical magnetic fields H_c, which overestimate the experimental values with about 10%. This is due to the fact that fluctuation corrections are not taken fully into consideration in the RPA calculations. Because of the mode softening at the K point, simple numerical procedures give unreliable results when calculating the induced magnetization and the quadrupole moment self-consistently. A semigraphical–seminumerical method has to be developed to determine the self-consistent solutions. The inclusion of correlation effects leads to a displacement of the minimum of the dispersion relation from the K point for magnetic fields close to H_c in $CsFeCl_3$. The experimentally detected incommensurable ordering in $CsFeCl_3$ in a magnetic field parallel to the z axis could be explained in this manner. The interplay between dipolar forces and correlation effects should define the precise position of the ordering vector for the incommensurability in the physical system. The correlation effects in $CsFeBr_3$ are not sufficiently large to cause the same effect in that material, in agreement with the experimental observations.

Predictions for the dynamical properties of correlation theory, which are based on Eq. (12), include the possibility of the occurrence of a central peak and a more complicated line-shape dependence of the excitation spectrum than the δ-function spectrum discussed in this paper, in particular when approaching the phase transition. The self-consistently renormalized δ-function spectrum indicates the best frequency consistent with the first frequency moments. In the presence of moderate line-shape broadening this is still a good measure for the peak position as observed by neutron scattering. However, for strongly damped modes the peak position no longer corresponds to the first moment frequency. This can be deduced by assuming, as is the natural first step, a damped harmonic oscillator line shape, see Refs. 4 and 23. The line shapes determined experimentally do not allow a fit to a more complicated function than the damped harmonic oscillator form, the two-pole line-shape function, and thus give no evidence for presence or absence of a central peak in the case of the soft-mode transition in a magnetic field parallel to the z axis. For a general discussion of line-shape effects more detailed theoretical and experimental studies are necessary.

ACKNOWLEDGMENTS

One of the authors (B.S.) would like to thank Risø National Laboratory for hospitality during which most of the manuscript was written. The authors are grateful to B. Dorner, M. Steiner, and D. Strauch for valuable discussions. P.A.L. wishes to thank the Institute Laue Langevin for hospitality during a visit there.

[1]Y.-L. Wang and B. R. Cooper, Phys. Rev. **172**, 539 (1968); **185**, 696 (1969); B. R. Cooper, in *Magnetic Properties of Rare Earth Metals,* edited by R. J. Elliott (Plenum, New York, 1972), p. 17.

[2]W. J. L. Buyers, T. M. Holden, E. C. Svensson, R. A. Cowley, and M. T. Hutchings, J. Phys. C **4**, 2139 (1971); I. Peschel, M. Klenin, and P. Fulde, *ibid.* **5**, L194 (1972); W. J. L. Buyers, in *Magnetism and Magnetic Materials—1974 (San Francisco),* Proceedings of the 20th Annual Conference on Magnetism and Magnetic Materials, edited by D. C. Graham, G. H. Lander, and J. J. Rhyne, AIP Conf. Proc. No. 24 (AIP, New York, 1975), p. 27.

[3]S. B. Hayley and P. Erdös, Phys. Rev. B **5**, 1106 (1972).

[4]P.-A. Lindgård, *Spin Waves and Magnetic Excitations,* edited by A. J. Borovik-Romanov and S. K. Sinha (North-Holland, New York, 1988), Vol. 22.1, Chap. 5.

[5]P.-A. Lindgård, J. Phys. C **8**, L178 (1975).

[6]P.-A. Lindgård, Phys. Rev. Lett. **50**, 690 (1983).

[7]S. K. Burke, W. G. Sterling, and K. A. McEwen, Phys. C **14**, L967 (1981).

[8]P.-A. Lindgård, Physica **120B**, 190 (1983).

[9]P.-A. Lindgård and O. G. Mouritsen, Phys. Rev. **41**, 688 (1990).

[10]B. Dorner, D. Visser, U. Steigenberger, K. Kakurai, and M. Steiner, Z. Phys. B **72**, 487 (1988); D. Visser, B. Dorner, and M. Steiner, Physica B **174**, 25 (1991).

[11]M. Steiner, X. X. Kakurai, W. Knop, B. Dorner, R. Pynn, U. Happek, P. Day, and G. McLeen, Solid State Commun. **38**, 1179 (1981).

[12]W. Knop, M. Steiner, and P. Day, J. Magn. Magn. Mater.

31-34, 1033 (1983); W. Knop, Ph.D. thesis, Technische Universität Berlin, 1985.
[13]H. Shiba, Solid State Commun. **44**, 511 (1982).
[14]B. Schmid, B. Dorner, D. Visser, and M. Steiner, Z. Phys. B **86**, 257 (1992).
[15]P.-A. Lindgård, J. Magn. Magn. Mater. **54-57**, 1227 (1986).
[16]H. Mori, Prog. Theor. Phys. **33**, 423 (1965); **34**, 399 (1965).
[17]J. H. Van Vleck, *Electric and Magnetic Susceptibilities* (Oxford, London, 1932).
[18]B. Dorner, D. Visser, and M. Steiner, Z. Phys. B **81**, 75 (1990).
[19]B. Schmid, B. Dorner, D. Visser, D. Petitgrand, and M. Steiner (unpublished).
[20]B. Schmid, B. Dorner, L. P. Regnault, D. Petitgrand, and M. Steiner (unpublished).
[21]S. K. Tyablikov, *Methods in the Quantum Theory of Magnetism* (Plenum, New York, 1967).
[22]L. D. Landau, and E. M. Lifshitz, *Statistical Physics,* translated by E. Peierls and R. F. Peierls (Addison-Wesley, Reading, MA, 1958).
[23]B. Dorner, *Coherent Inelastic Neutron Scattering in Lattice Dynamics,* edited by G. Höhler, Springer Tracts in Modern Physics, Vol. 93 (Springer-Verlag, Berlin, 1982); B. Fåk and B. Dorner (unpublished).